Neon Matrix Infrared Spectra and DFT Calculations of Tungsten Hydrides WH_x ($x = 1-4, 6$)

Xuefeng Wang and Lester Andrews*

Department of Chemistry, University of Virginia, Charlottesville, Virginia 22904-4319

Received: April 10, 2002; In Final Form: May 31, 2002

Laser-ablated tungsten atoms react with molecular hydrogen upon condensation in excess neon. The tungsten hydrides WH, WH_2, WH_3, WH_4, and WH_6 are identified by isotopic substitution (D_2, HD) and by density functional theory calculations of vibrational fundamentals. The WH diatomic gives a 1860.2 cm^{-1} band, WH_2 gives a strong 1831.9 cm^{-1} absorption, and WH_3 gives a sharp 1894.6 cm^{-1} peak. Absorptions due to WH_4 appear at 1920.1 and 525.2 cm^{-1}, increase on annealing in solid neon, and support a tetrahedral structure. Sharp new absorptions at 2021.2, 2004.4, 1953.8, 1927.5, 1080.3, and 840.7 cm^{-1} are assigned to WH_6, based on deuterium isotopic shifts and comparison with frequencies computed by DFT for the distorted trigonal prism structure predicted earlier to be the global minimum energy structure for WH_6. The bands of WH_6 increase on annealing, decrease on broadband photolysis, and restore on further annealing. This is the first experimental identification of the WH_2, WH_4, and WH_6 hydride molecules, and WH_6 is the only known neutral metal hexahydride.

Introduction

Tungsten hydrides and tungsten dihydrogen complexes continue to be of interest because of their roles in catalytic hydrogenation processes and the rationalization of molecular structures. Tungsten hydrides are used in hydride-transfer reactions,[1,2] and the isotopic effects for a series of $L(CO)_3WH$ and $L(CO)_3WD$ compounds have been measured.[3] The compound $Cp(CO)_3WH$ exhibits a W−H(D) frequency at 1845 (1326) cm^{-1} in hexane solution, which provides a benchmark for isolated tungsten hydride molecules. The $Cp(CO)_3WH$ hydride has also been used as a building block to prepare metal clusters.[4] The discovery of the first isolable molecular hydrogen complexes with a tungsten metal center,[5] $W(CO)_3(PR_3)_2(\eta^2\text{-}H_2)$ (R = Cy and *i*-Pr), promoted extensive theoretical and experimental investigations of H−H bond activation on transition metal centers.[6−10] In particular, dihydrogen complexes of group 6 transition metal carbonyls of the form $M(CO)_x(H_2)_y$ are of special significance as chemical intermediates.

The hexamethyltungsten molecule, $W(CH_3)_6$, has been synthesized, and it is particularly important for understanding the bonding in transition metal compounds.[11] In the gas-phase, $W(CH_3)_6$ is not octahedral as might be expected from valence shell electron pair repulsion (VSEPR),[12] but the electron diffraction pattern has been interpreted using a distorted trigonal prismatic D_{3h} structure, and a low-temperature single-crystal X-ray diffraction investigation revealed further distortion to C_{3v} symmetry.[13,14] Later theoretical calculations[15] show that the equilibrium structure of $W(CH_3)_6$ has C_3 symmetry with local C_{3v} symmetry for the WC_6 skeleton in quantitative agreement with the X-ray diffraction results.[14] For tungsten hexahydride (WH_6), theoretical calculations agree that the octahedral structure predicted by VSEPR is considerably (>100 kcal/mol) higher in energy than lower symmetry structures and that the global minimum energy structure is an eclipsed distorted trigonal prism (C_{3v}), which is the same basic structure computed for $W(CH_3)_6$.[15−18] However, there is no experimental data on WH_6, which is predicted to be fluxional from low barrier heights computed for interconversion of low-energy isomeric structures.[18]

Several metal hydrides and metal hydrogen complexes have been characterized for Cr and Mo in matrix isolation experiments.[19,20] However, the reaction of tungsten has not yet been investigated because tungsten is very hard to vaporize using traditional methods. Laser ablation is one of the most promising techniques for evaporating high-melting metals. Using laser ablation, metal atoms are produced with minimum heat load on the matrix. The tungsten atoms react with H_2 during condensation of the matrix, and as a result, metal hydrides and hydrogen complexes can be synthesized and trapped for spectroscopic study.[21−23] Using laser ablation, the metal polyhydrides, TiH_4, ZrH_4, and HfH_4, with T_d structure,[24−26] and metal hydride hydrogen complexes, $(H_2)RhH_2$, $(H_2)RhH_3$, and $(H_2)AuH$, have been identified in neon and argon matrixes by infrared spectroscopy and reproduced by theoretical calculations.[27,28]

We present here a matrix isolation investigation of laser-ablated tungsten atom reactions with dihydrogen. The tungsten hydride molecules $WH_{1-4,6}$ are characterized by matrix infrared spectroscopy and density functional theory (DFT) frequency calculations. Our results on WH_6 have appeared in a brief communication.[29] The observation of higher hydrides provides important molecular structure information for better understanding of bonding in transition metal polyhydrides and polyhydrogen complexes.

Experimental and Computational Methods

The experiment for reactions of laser-ablated tungsten atoms with small molecules during condensation in excess argon and neon has been described in detail previously.[30,31] The Nd:YAG laser fundamental (1064 nm, 10 Hz repetition rate with 10 ns

* To whom correspondence should be addressed. E-mail: lsa@virginia.edu.

10.1021/jp025920d CCC: $22.00
Published on Web 06/29/2002

TABLE 1: Infrared Absorptions (cm^{-1}) Observed from Reactions of Tungsten and Dihydrogen in Excess Argon, Neon, and Deuterium

argon			neon			deuterium	
H_2	HD	D_2	H_2	HD	D_2	pure D_2	identification
			2021.2[b]	2003.4			WH_6
			2004.4[b]	1432.5	1439.9		WH_6
			1953.8[b]	1952.6			WH_6
1923.7			1927.5[b]	1927.5	1384.1		WH_6
			1925.7[c]	1925.7			$[WH_4]$[e]
(1911)		(1374)	1921.8[d]	1935.7	1377.8	1377.7	WH_4 (site)
			1920.5[d]	1384.8	1377.0		WH_4
1866.2[a]	1865.7	1337.7	1911.5[c]	1909.7	1371.2		$[WH_4]$[e]
			1909.9[c]	1371.2	1370.3		$[WH_4]$[e] (site)
1878.6	1883.5	1344.3	1895.3	1901.2	1361.1		WH_3
	1348.4		1894.6	1363.6	1357.7		WH_3 (site)
1852.6		1327.6	1860.2	1860.0	1334.0	1334.8	WH
(1816.8)			1831.9	1839.7	1323.9	1325.3, 1323.2,	WH_2
				1330.3		1322.7, 1321.1	
			1786	1783	1287	1288, 1283	W_xH_y
			1735		1250	1248	W_xH_y
			1080.3[b]	797.9	779.2		WH_6
			995.8		716.4	718.9	$(WH)_2$
			840.7[b]		609.1		WH_6
			709.4		510.9	512.2	?
			526.9[d]				WH_4
			525.2[d]				WH_4 (site)
			515.6[c]				$[WH_4]$[e]
			514.0[c]				$[WH_4]$[e] (site)

[a] More likely $(H_2)_xWH_2$ complex. [b] Relative integrated band absorbances are 3, 40, 12, 100, 30, and 14, respectively, highest to lowest frequency. [c] Relative integrated band intensities are 6, 100, and 60, respectively. [d] Relative integrated band intensities are 100 and 33, respectively. [e] $[WH_4]$ denotes perturbed WH_4, i.e., $(WH_4)(Ne)_x(H_2)$.

pulse width) was focused onto a rotating tungsten target (Johnson-Matthey, 99.95%). The laser energy was varied from 5 to 40 mJ/pulse. Laser-ablated tungsten atoms were co-deposited with hydrogen molecules (0.2−6%) in excess neon or argon onto a 3.5 K CsI cryogenic window at 2−4 mmol/h for 1 h using a Sumitomo Heavy Industries model RDK-205D cryocooler. Hydrogen (Mathenson), D_2 (Liquid Carbonic), HD (Cambridge Isotopic Laboratories), and $H_2 + D_2$ mixtures were used in different experiments. FTIR spectra were recorded at 0.5 cm^{-1} resolution on a Nicolet 750 with 0.1 cm^{-1} accuracy using an MCTB detector. Matrix samples were annealed at different temperatures, and selected samples were subjected to broadband photolysis by a medium-pressure mercury arc lamp (Phillips, 175W) with the globe removed (240−700 nm).

Density functional theoretical calculations of tungsten hydrides and tungsten hydride hydrogen complexes were done for comparison. The Gaussian 98 program[32] was employed to calculate the structures and frequencies of expected molecules using the BPW91 and B3LYP functionals.[33,34] The 6-311++G-(d,p) basis set for hydrogen and Los Alamos ECP plus DZ and SDD pseudopotentials for tungsten atom were used.[35−37] All of the geometrical parameters were fully optimized, and the harmonic vibrational frequencies were obtained analytically at the optimized structures.

Results

Matrix-isolation infrared spectra are presented for tungsten atom reactions with H_2, D_2, and HD in excess neon, pure deuterium, and argon. Density functional theoretical calculations of tungsten hydrides and hydrogen complexes are given for comparison.

Laser-Ablated Tungsten Atom Reactions. Figure 1 illustrates infrared spectra for three 4% H_2 in neon matrix samples using different laser energies for tungsten ablation and reaction during deposition. The first ablation gave a barely observable

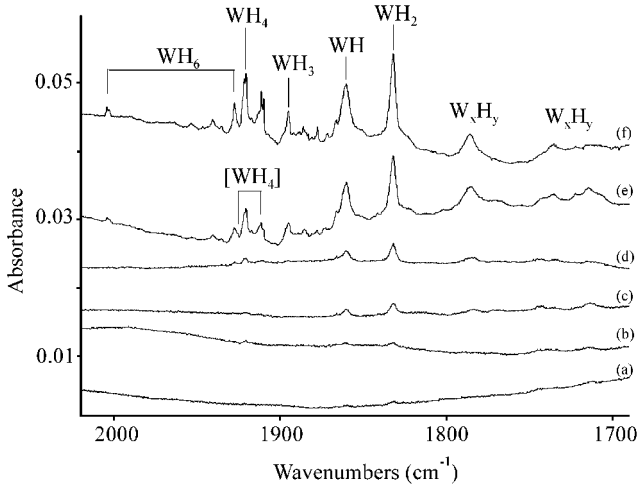

Figure 1. Infrared spectra in the 2020−1690 cm^{-1} region for tungsten ablated at three different laser energies and co-deposited with 4% H_2 in neon at 3.5 K: (a) low laser energy co-deposited sample, (b) after annealing to 8 K, (c) medium laser energy co-deposited sample, (d) after annealing to 8 K, (e) high laser energy co-deposited sample, and (f) after annealing to 8 K.

blue plume on the target surface, the second was approximately double the first plume intensity, and the third doubled again the plume intensity: these experiments employed progressively increasing tungsten atom concentrations. The spectra in Figure 1 show increasing absorption band intensities with increasing W atom concentrations. Broader absorptions at 1786, 1735, and 1715 cm^{-1} appear to have a higher order dependence on metal and are thus due to polymetal hydride species that cannot be identified here. New sharp 1831.9, 1860.2, 1920.5, and 1927.5 cm^{-1} absorptions are observed with low W atom concentrations, and they maintain constant relative intensities with increasing W at constant H_2 concentration. The 1831.9 cm^{-1} band increases

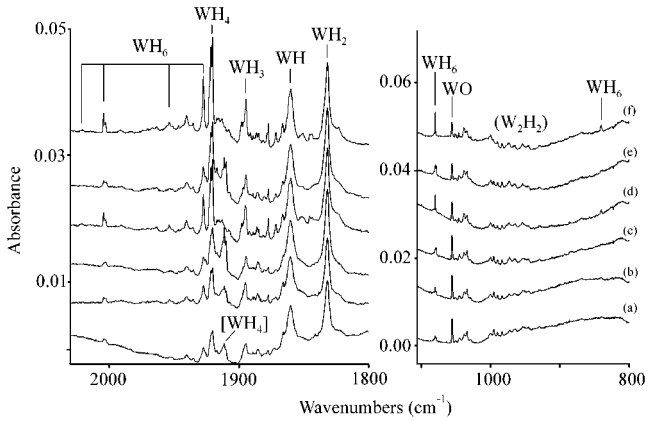

Figure 2. Infrared spectra in the 2030−1800 and 1100−800 cm^{-1} regions for laser-ablated tungsten co-deposited with 4% H_2 in neon at 3.5 K: (a) sample co-deposited for 1 h, (b) after annealing to 8 K, (c) after broadband (240−700 nm) photolysis for 20 min, (d) after annealing to 10 K, (e) after broadband photolysis for 15 min, and (f) after annealing to 11 K.

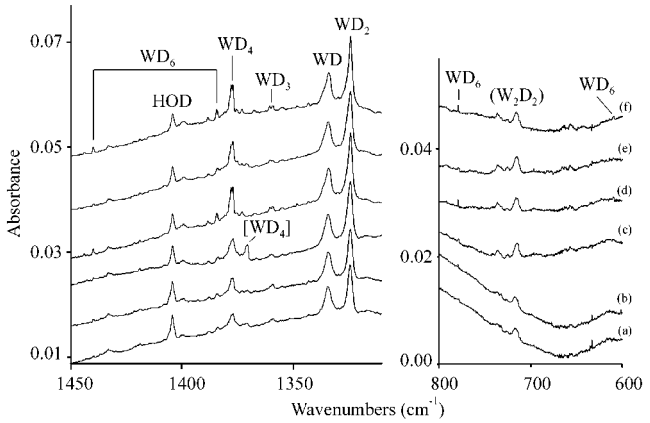

Figure 3. Infrared spectra in the 1450−1310 and 800−600 cm^{-1} regions for laser-ablated tungsten co-deposited with 4% D_2 in neon at 3.5 K: (a) sample co-deposited for 1 h, (b) after annealing to 8 K, (c) after broadband (240−700 nm) photolysis for 20 min, (d) after annealing to 10 K, (e) after broadband photolysis for 15 min, and (f) after annealing to 11 K.

on photolysis, and the 1927.5 and 1920.5 cm^{-1} bands increase on annealing.

Figure 2 shows the spectra for the highest laser energy ablated tungsten atom co-deposition with 4% H_2 in solid neon, and the absorptions are listed in Table 1. After deposition, new bands at 1920.5, 1911.5, 1894.6, 1860.2, and 1831.9 cm^{-1} and a group of five weak absorptions at 2004.4, 1953.8, 1927.5, 1080.3, and 840.7 cm^{-1} were observed. Stepwise annealing to 7 and 10 K increased the 1920.5 cm^{-1} band, and the five weak absorptions with a weaker associated 2021.2 cm^{-1} peak, but a 15 min broadband photolysis decreased this group and produced a sharp new band at 1911.5 cm^{-1} and an associated band at 515.6 cm^{-1} (not shown). However, the six bands recovered on further annealing to 11 K at the expense of the 1911.5 and 515.6 cm^{-1} bands.

The spectra for reaction products of tungsten atoms with D_2 are similar, but shifted to lower wavenumbers, as shown in Figure 3, and the absorptions are also listed in Table 1. Reactions with HD gave some of the above absorptions, and several new peaks, as illustrated in Figure 4.

The spectra of laser-ablated W atoms in pure deuterium with higher laser energy are illustrated in Figure 5. Strong absorptions observed at 1334.8 and 1322.7 cm^{-1} are near the strongest two bands observed for 5% D_2 in neon.

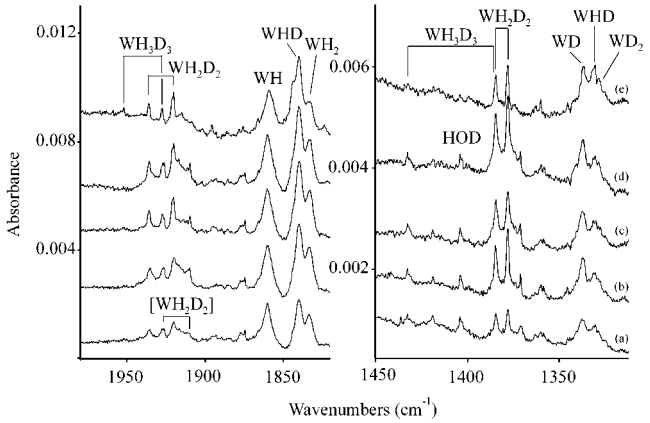

Figure 4. Infrared spectra in the 1970−1820 and 1450−1310 cm^{-1} regions for laser-ablated tungsten co-deposited with 2% HD in neon at 3.5 K: (a) sample co-deposited for 1 h, (b) after annealing to 8 K, (c) after broadband (240−700 nm) photolysis for 20 min, (d) after annealing to 9K, and (e) after annealing to 11 K.

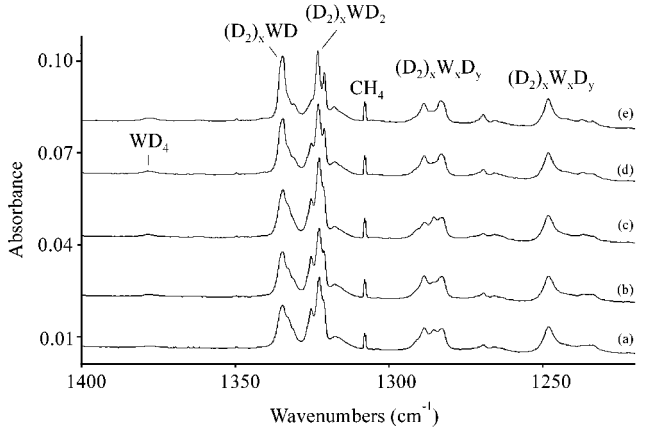

Figure 5. Infrared spectra in the 1400−1220 cm^{-1} region of pure deuterium co-deposited with laser-ablated tungsten at 3.5 K: (a) sample deposited for 25 min, (b) after annealing to 6 K, (c) after broadband photolysis for 10 min, and (d) after annealing to 8 K.

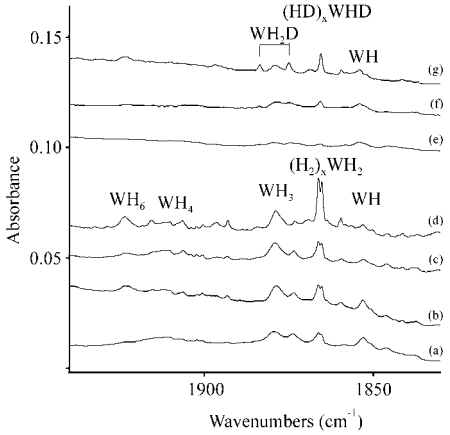

Figure 6. Infrared spectra in the 1940−1830 cm^{-1} region for laser-ablated tungsten co-deposited with 2% H_2 in argon at 3.5 K: (a) sample co-deposited for 1 h, (b) after annealing to 17 K, (c) after broadband photolysis for 15 min, and (d) after annealing to 25 K.

Argon matrix spectra of tungsten atom and hydrogen molecule reaction products are shown in Figure 6. Major absorptions at 1878.7, 1866.2, and 1852.7 cm^{-1} were observed after deposition. Annealing to 17 K increased all bands including weaker 1923.7 and 1911 cm^{-1} absorptions. Broadband photolysis decreased the 1866.2 cm^{-1} band, but the 1866.2 and 1923.7 cm^{-1} bands

TABLE 5: Calculated Geometries, Vibrational Frequencies (cm^{-1}), and Intensities (km/mol) for WH_4 ($^3A_1$, T_d)

method	geometry (Å,deg)	frequencies, cm^{-1} (modes, intensities, km/mol)
BPW91/6-311++G(d,p)/ SDD	WH,1.712	WH_4: 1982.8(a_1,0), 1955.2(t_2,175 × 3), 658.9(e,0), 558.4(t_2,98 × 3) WD_4: 1402.6(a_1,0), 1388.5(t_2,90 × 3), 466.1(e,0), 397.6(t_2,49 × 3) WH_2D_2: 1969.1(84), 1954.9(172), 1395.6(48), 1389.0(93), 618.1(33), 570.1(0), 522.1(85), 442.8(62), 422.4(62)
BPW91/6-311++G(d,p)/ LanL2DZ	WH,1.695	WH_4: 2003.7(a_1,0), 1957.1(t_2,161 × 3), 681.7(e,0), 574.3(t_2,98 × 3). WD_4: 1417.3(a_1,0), 1389.9(t_2,89 × 3), 482.2(e,0), 408.9(t_2,50 × 3) WH_2D_2: 1980.9(76), 1956.9(158), 1403.2(46), 1390.3(85), 638.5(33), 590.4(0), 537.4(85), 456.0(62), 435.1(41)
B3LYP/6-311++G(d,p)/ SDD	WH,1.712	WH_4: 2005.1(a_1,0), 1971.6(t_2,233 × 3), 673.3(e,0), 568.6(t_2,107 × 3) WD_4: 1418.4(a_1,0), 1400.2(t_2,118 × 3), 476.3(e,0), 404.9(t_2,54 × 3) WH_2D_2: 1988.5(110), 1971.1(226), 1409.2(64), 1400.9(123), 631.0(36), 582.6(0), 531.6(93), 451.0(68), 430.6(45).
B3LYP/6-311++G(d,p)/ LanL2DZ	WH,1.694	WH_4: 2033.9(a_1,0), 1981.3(t_2, 231 × 3), 696.5(e, 0), 585.9(t_2, 113 × 3) WD_4: 1438.7(a_1, 0), 1407.0(t_2, 118 × 3), 492.7(e, 0), 417.2(57 × 3) WH_2D_2: 2008.2(108), 1980.9(227), 1422.3(67), 1407.6(123), 652.1(37), 603.3(0), 548.3(98), 465.4(71), 444.1(48)

[a] $(H_2)WH_2$ with $^5A'$ (C_s), $^5B(C_2)$, and $^5A_1$ (C_{2v}, planar) states are 24.7, 30.1, and 43.0 kcal/mol higher in energy than WH_4 ($^3A_1$, T_d) at this level of theory and have one imaginary deformation frequency.

TABLE 2: Calculated Bond Lengths, Harmonic Vibrational Frequencies (cm^{-1}), and Intensities (km/mol) for WH and WD in the Ground $^6\Sigma^+$ State at Different Levels of Theory[a]

method	bond(Å)	frequencies, cm^{-1} (intensities, km/mol)
BPW91/6-311++G(d,p)/SDD	1.715	WH: 1915.4(89); WD: 1358.6(45)
BPW91/6-311++G(3df,3pd)/SDD	1.714	WH: 1911.1(84); WD: 1354.8(42)
BPW91/6-311++G(d,p)/LanL2DZ	1.702	WH: 1930.1(83): WD: 1369.0(42)
BPW91/6-311++G(3df,3pd)/LanL2DZ	1.701	WH: 1955.9(92): WD: 1387.4(46)
B3LYP/6-311++G(d,p)/SDD	1.720	WH:1920.1(112); WD: 1361.9(57)
B3LYP/6-311++G(d,p)/LanL2DZ	1.706	WH:1934.3(105); WD: 1372.0(53)

[a] CAS and MCSCF calculations, ref 38, give 1.727 Å and 1897 cm^{-1} for WH.

TABLE 3: Calculated Geometries, Vibrational Frequencies, and Infrared Intensities for WH_2 ($^5B_2$, C_{2v}) at Different Levels of Theory[a]

method	geometry (Å,deg)	frequencies, cm^{-1} (modes, intensities, km/mol)
BPW91/6-311++G(d,p)/SDD[b]	WH,1.717; HWH,112.9	WH_2: 1928.0(a_1,50), 1921.9(b_2,183), 640.9(a_1,42) WD_2: 1366.4(a_1,25), 1364.7(b_2,93), 455.0(a_1,21) WHD: 1924.8(115), 1365.8(61), 555.2(34)
BPW91/6-311++G(3df,3pd)/SDD	WH,1.717; HWH,113.0	WH_2: 1921.9(a_1,45), 1915.9(b_2,170), 642.2(a_1,42) WD_2: 1362.0(a_1,23), 1360.4(b_2,86), 455.9(a_1,21) WHD: 1918.7(106), 1361.5(56), 556.2(33)
BPW91/6-311++G(d,p)/LanL2DZ	WH,1.700; HWH,112.1	WH_2: 1943.8(a_1,47), 1920.5(b_2,163), 639.9(a_1,46) WD_2,: 1377.6(a_1,24), 1363.6(b_2,82), 454.2(a_1,23) WHD: 1932.2(103), 1370.6(56), 554.4(37)
BPW91/6-311++G(3df,3pd)/LanL2DZ	WH,1.704; HWH,113.3	WH_2: 1969.7(a_1,44), 1946.3(b_2,181), 648.2(a_1,41) WD_2,: 1395.9(a_1,22), 1382.0(b_2,91), 460.2(a_1,21) WHD: 1958.0(110), 1389.1(60), 561.4(33)
B3LYP/6-311++G(d,p)/SDD	WH,1.720; HWH,113.0	WH_2: 1933.9(a_1,72), 1925.8(b_2,239), 643.8(a_1,49) WD_2: 1370.6(a_1,37), 1367.4(b_2,121), 456.9(a_1,25) WHD: 1929.7(154), 1369.4(81), 557.6(40)
B3LYP/6-311++G(d,p)/LanL2DZ	WH,1.703; HWH,112.3	WH_2: 1954.6(a_1,69), 1930.8(b_2,217), 647.7(a_1,52) WD_2: 1385.2(a_1,35), 1370.9(b_2,110), 459.7(a_1,26) WHD: 1942.7(139), 1378.2(76), 561.4(42)

[a] CAS and MCSCF calculations, ref 39, give 1.763 Å and 118.1° for WH_2. [b] WH_2 with linear structure ($^5\Sigma_u$) lies 53.6 kcal/mol higher in energy.

increased markedly on further annealing. Notice that the band intensity distribution is different in solid argon and neon.

Calculations. The WH and WH_2 molecules have $^6\Sigma^+$ and $^5B_2$ ground electronic states, respectively, in our calculations (Tables 2 and 3), which are in agreement with higher level calculations.[38,39] The H−W−H bond angle in WH_2 is predicted to be 113°, which is about 10° larger than in CrH_2. The same ground states are computed for CrH and CrH_2.[40−42]

For WH_3 and $(H_2)WH$, we investigated equilibrium structures with various electronic states. WH_3 has the pyramidal (C_{3v}) structure and $^4A_1$ ground state (Table 4), which are in agreement with a recent CCSD(T) ab initio study.[43] The side-on $(H_2)WH$ conformation has the $^6A_1$ ground state, which is formed by H_2 reacting with the WH ($^6\Sigma^+$). The dihydrogen bonding energy for $(H_2)WH$ is 2.8 kcal/mol at the BPW91/6-311++G**/LanL2DZ level. However, $(H_2)WH$ is 21.3 kcal/mol higher in energy than WH_3.

WH_4 is calculated to have a $^3A_1$ ground state with tetrahedral molecular shape, Table 5, which is the global minimum energy, in disagreement with a D_{2d} structure determined by symmetry analysis.[44] The $WH_2(H_2)$ species does not exist on the triplet potential energy surface, because the H_2 moiety dissociates in the optimization process and leads to the tetrahydride WH_4. However, optimization under C_s, C_2, and C_{2v} symmetry constraints with quintet electronic states gives dihydride hydrogen complexes, $WH_2(H_2)$, at the BPW91 level of theory, which are higher in energy by 24.7, 30.1, and 43.0 kcal/mol, respectively. The most important feature for these $WH_2(H_2)$

TABLE 4: Calculated Geometries, Vibrational Frequencies (cm^{-1}), and Intensities (km/mol) for WH_3 ($^4A_1$, C_{3v})

method	geometry (Å,deg)	frequencies, cm^{-1} (modes, intensities, km/mol)
BPW91/ 6-311++G(d,p)/SDD	WH,1.716 HWH,112.8	WH_3: 1945.9(a_1,17), 1932.9(e,186 × 2), 717.5(e,30 × 2),381.4(a_1,108). WD_3: 1377.5(a_1,9), 1372.7(e,94 × 2), 509.1(e,15 × 2), 271.8(a_1,55). WH_2D; 1941.6(72), 1932.6(185), 1374.8(70), 709.6(33), 596.9(17), 347.6(91) WHD_2: 1936.9(127), 1375.9(38), 1373.2(97), 646.4(27), 522.0(14), 309.9(72)
BPW91/6-311++G(d,p)/ LanL2DZ	WH,1.700; HWH,112.1	WH_3: 1966.8(a_1,17), 1936.0(e,177 × 2), 715.5(e,34 × 2), 415.9(a_1,116). WD_3: 1392.3(a_1,9), 1374.9(e,90 × 2), 507.6(e,17 × 2), 296.3(a_1,59). WH_2D: 1956.8(68), 1935.8(175), 1380.7(68), 699.8(38), 598.2(20), 384.7(98) WHD_2: 1946.3(119), 1386.2(38), 1375.1(92), 639.6(32), 521.4(16), 340.8(77)
B3LYP/6-311++G(d,p)/ SDD	WH,1.718; HWH,112.2	WH_3: 1964.8(a_1,27), 1947.0(e,242 × 2), 700.8(e,34 × 2),404.7(a_1,132). WD_3: 1390.9(a_1,14), 1382.8(e,123 × 2), 497.2(e,17 × 2), 288.3(a_1,67). WH_2D; 1958.9(97), 1946.7(240), 1386.1(92), 692.5(38), 583.8(19), 368.6(112) WHD_2: 1952.7(166), 1388.2(52), 1383.4(126), 630.5(32), 511.3(16), 328.4(88)
B3LYP/6-311++G(d,p)/ LanL2DZ	WH,1.700; HWH,112.1	WH_3: 1989.3(a_1,27), 1954.9(e,237 × 2), 699.4(e,38 × 2), 427.9(a_1,142) WD_3: 1408.3(a_1,14), 1388.3(e,121 × 2), 496.2(e,19 × 2), 304.9(a_1,72) WH_2D: 1978.0(93), 1954.6(223), 1395.3(87), 690.5(40), 583.6(21), 390.2(120) WHD_2: 1966.3(161), 1401.4(53), 1388.8(118), 628.2(36), 512.4(18), 347.2(94).

[a] $(H_2)WH$ calculated at this level is 21.3 kcal/mol higher in energy than WH_3; WH, 1.723; WH′, 2.160; H′H′, 0.786; 3730.9 (a_1, 104), 1893.9 (a_1, 190), 921.9 (b_2, 14), 557.5 (a_1, 2), 382.6 (b_1, 7), 357.1 (b_2, 14).

TABLE 6: Calculated Geometries, Vibrational Frequencies, and Infrared Intensities (km/mol) for WH_5 (C_s, $^2A'$)

method	geometry (Å,deg)	frequencies, cm^{-1} (modes, intensities, km/mol)
BPW91/6-311++G(d,p)/ SDD	WH, 1.728[a] WH′, 1.706[b] WH″, 1.684 HWH, 115.1 HWH″, 115.7	WH_5: 2029.8(a′,63), 2016.6(a″,126), 1970.5(a′,69), 1959.8(a′,95), 1930.1(a′,191), 1009.4(a′,41), 910.1(a″,28), 900.6(a′,2), 820.1(a″,28), 750.8(a′,28), 547.6(a′,65), 411.9(a″,1)
BPW91/6-311++G(d,p)/ LanL2DZ[a]	WH, 1.710 WH′, 1.690 WH″, 1.670 HWH′ 115.2 HWH″ 115.4	WH_5: 2035.9(35), 2018.0(75), 1980.8(74), 1963.4(117) 1930.3(186), 1017.5(42), 919.5(29), 912.0(2), 835.4(28), 765.2(29), 553.7(69), 414.2(1)

[a] $(H_2)WH_3$ ($^4B_2$, C_{2v}) lies 16.6 kcal/mol higher in energy. [b] $(H_2)_2WH$ ($^4A''$, C_s) lies 29.0 kcal/mol higher in energy.

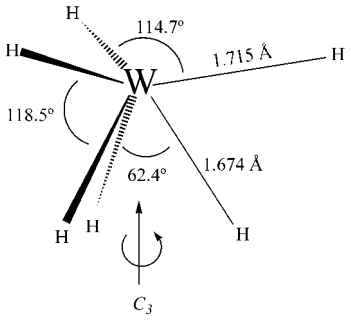

Figure 7. Distorted trigonal prismatic C_{3v} structure optimized for WH_6 using BPW91/6-311++G(d,p)/SDD.

complexes is one imaginary frequency indicating a transition state to the higher T_d symmetry conformation.

Doublet, quartet, and sextet electronic states were extensively examined for WH_5, and a low-spin $^2A'$ state with C_s symmetry is found to be the ground state (Table 6). The high-spin $WH(H_2)_2$ ($^4A''$) species containing two H_2 moieties is located as a minimum on the potential energy surface at 29.0 kcal/mol higher in energy (BPW91 level) compared with WH_5 ($^2A'$). The $WH_3(H_2)$ complex was also considered and geometry optimization converged to a transition state ($^4B_2$).

The structures calculated for WH_6 are listed in Table 7, and the ground state $^1A_1$ structure is shown in Figure 7. Schaefer and co-workers[16] investigated tungsten hexahydride (WH_6) and suggested that the ground state is a distorted trigonal prism with C_{3v} symmetry, which is far from the octahedral structure based on the VSEPR model.[12] In addition, two other singlet structures (distorted C_{3v} structure and C_{5v} pentagonal pyramid) were characterized as higher energy minima, and another C_{5v} minimum with an umbrella-like structure was located.[17] Meanwhile DFT calculations have been performed, and all studies agree on the global minimum.[18] In this work, we use DFT calculations to predict frequencies of these structures to help assign the neon matrix vibrational frequencies due to WH_6. Additionally, another isomer of WH_6, the high-spin hydrogen complex $WH_2(H_2)_2$ ($^3A''$), is predicted as a fifth minimum, which is 26.0 kcal/mol higher in energy than ground-state C_{3v} WH_6 at the BPW91/6-311++G**/SDD level of theory. However, $WH_4(H_2)$ complexes decomposed on both singlet and triplet surfaces.

Discussion

WH. A band centered at 1860.0 cm^{-1} was observed in H_2, $H_2 + D_2$, and HD neon matrix experiments, whereas a 1334.0 cm^{-1} band appeared with D_2 (H/D isotopic frequency ratio 1.394). These bands are appropriate for the diatomic molecules WH and WD. In solid argon, the stretching frequencies of WH and WD were identified at 1852.6 and 1327.6 cm^{-1}, respectively, which show essentially the same 1.395 H/D isotopic ratio and constitute a reasonable matrix shift.[31,45]

Our DFT frequency calculations for diatomic WH are summarized in Table 2. The BPW91/6-311++G**/SDD calculation predicted the ground state $^6\Sigma^+$ WH fundamental at 1915.4 cm^{-1}, which requires a 0.971 scale factor to fit the 1860 cm^{-1} neon matrix measurement. The B3LYP functional with

TABLE 7: Calculated Geometries, Vibrational Frequencies, and Intensities for WH_6

molecule (state, symmetry)	geometry (Å,deg)	relative energy (kcal/mol)	frequencies, cm^{-1} (modes, intensities/km/mol)
BPW91/6-311++G(d,p)/ SDD			
WH_6 (prism)	WH,1.715	0.0	2059.3(a_1,45), 2039.9(e,72 × 2), 1963.7(a_1,92),
($^1A_1$, C_{3v})	WH′,1.674		1949.8(e,141 × 2), 1155.1(a_1,101), 946.1(e,14ξ2),
	HWH,114.7		894.0(e,60 × 2), 805.8(a_2,0), 758.6(a_1,10),
	H′WH′,62.4		709.5(e,9 × 2)
			[1464.9, 1446.9, 1389.9, 1383.7, 717.6, 672.4, 632.4, 570.0, 541.0, 503.5][a]
WH_6 (parachute)	WH,1.736	0.3	2029.5(a_1,28), 2018.4(e,190 × 2), 1984.7(e,0 × 2),
($^1A_1$, C_{5v})	WH′,1.688		1924.4(a_1,201), 1072.5(e,0 × 2), 980.4(a_1,3),
	HWH′,115.0		913.7(e,96 × 2), 763.9(e,5 × 2), 692.3(e,0 × 2)
WH_6 (hemisphere)	WH,1.706	9.2	2093.8(a_1,20), 2078.3(e,52 × 2), 1966.5(a_1,40),
($^1A_1$, C_{3v})	WH′,1.660		1964.9(e,163 × 2), 1131.6(a_1,118), 1085.9(e,83 × 2),
	HWH,118.6		899.7(e,39 × 2), 793.5(e,0 × 2), 727.9(a_1,38),
	H′WH′,61.8		574.0(a_2,0)
WH_6 (umbrella)	WH,1.649	16.7	2125.3(a_1,12), 2031.0(a_1,1), 2024.0(e1,215 × 2),
($^1A_1$, C_{5v})	WH′,1.688		1993.2(e_2,0 × 2), 1119.7(e_2,0 × 2), 1062.3(e_1,206 × 2),
	HWH′,65.2		1020.8(a_1,13), 746.6(e_1,0 × 2), 665.9(e_2,0 × 2)
$WH_2(H_2)_2$	WH,1.714	26.0	2456.5(a′,1), 2336.7(a″,812), 1944.2(a′,44),
($^3A''$, C_s)	WH′(H′),1.828		1941.5(a′,259), 1856.8(a′,18), 1747.3(a″,0), 1326.3(a′,1),
	H′H′,0.909		797.5(a″,178), 747.5(a′,19), 680.4(a″,0), 627.8(a′,69),
	HWH,120.2		471.6(a″,0), 456.9(a″,570), 418.2(a′,16), 408.9(a′,40)
	H′WH′,167.7		[1737.7(0), 1656.6(401), 1378.6(122),
			1377.3(25), 1315.7(13), 1236.0, ...][a]
			[2082.1(19), 2079.6(512), 1942.0(144),
			1600.4(8), 1448.1(146), 1378.6(173), ...][b]
B3LYP/6-311++G(d,p)/SDD			
WH_6 (prism)	WH,1.715	0.0	2094.6(a_1,49), 2066.7(e,99 × 2), 1991.2(a_1,125),
($^1A_1$, C_{3v})	WH′,1.671		1970.3(e,166 × 2), 1173.9(a_1,120), 941.1(e,16 × 2),
	HWH,113.9		890.8(e,65 × 2), 825.3(a_2,0), 768.1(a_1,14),
	H′WH′,63.0		692.0(e,14 × 2)
			[1489.8, 1466.3, 1409.7, 1397.9, 830.9, 668.9,
			630.2, 583.8, 548.1, 491.0][a]
WH_6 (parachute)	WH,1.734	−0.1	2065.2(a_1,30), 2046.5(e_1,238 × 2), 2003.2(e_2,0 × 2),
($^1A_1$, C_{5v})	WH′,1.685		1961.5(a_1,253), 1091.2(e_2,0 × 2), 976.0(a_1,3),
	HWH′,114.6		921.7(e_1,111 × 2), 768.8(e_1,7 × 2), 692.3(e_2,0 × 2)
WH_6 (hemisphere)	WH,1.709	11.9	2129.3(a_1,21), 2105.7(e,65 × 2), 1979.1(a_1,57),
($^1A_1$, C_{3v})	WH′,1.656		1974.3(e,206 × 2), 1139.6(a_1,130), 1079.7(e,93 × 2),
	HWH,119.2		875.8(e,45 × 2), 782.1(e,0 × 2), 730.8(a_1,54),
	H′WH′,61.5		501.5(a_2,0)
WH_6 (umbrella)	WH,1.643	21.5	2162.1(a_1,11), 2054.1(a_1,2)), 2040.5(e_2,273 × 2),
($^1A_1$, C_{5v})	WH′,1.679		2001.2(e_2,0 × 2), 1126.2(e_2,0 × 2), 1041.4(e_1,243 × 2),
	HWH′,66.1		1001.2(a_1,5), 749.0(e_1,0 × 2), 629.1(e_2,0 × 2)
$WH_2(H_2)_2$	WH,1.717	25.0	2742.8 (a′,0), 2602.1(a″,1043), 1949.7(a′,65),
($^3A''$, C_s)	WH′(H′),1.847		1943.7(a′,345), 1828.9(a′,27), 1717.7(a″,0),
	H′H′,0.871		1282.3(a′,0),811.6(a″,231), 723.5(a′,28),
	HWH,119.6		666.0(a″,0), 623.9(a′,90), 522.7(a″,422),
	H′WH′,169.9		518.3(a″,21), 432.1(a′,18), 370.7(a′,25)

[a] WD_6 frequencies. [b] $WHD(HD)_2$ frequencies.

the same basis sets gives almost the same W−H frequency at 1920.1 cm^{-1}. However, both functional calculations with the LanL2DZ pseudopotential give slightly higher frequencies. The BPW91 functional and SDD pseudopotential match our experimental value better.

The 1860 cm^{-1} neon matrix fundamental is in excellent agreement with the infrared spectra of a series of $L(CO)_3WH$ hydrides in hexane solution, which exhibit W−H stretching frequencies in the 1854−1827 cm^{-1} region and H/D isotopic frequency ratios in the 1.391−1.394 range.[3] A low-resolution 680 nm emission spectrum from a tungsten discharge source has been attributed to WH.[46] However, the deduced frequency (531 ± 62 cm^{-1}) and deuterium counterpart (145 ± 144 cm^{-1}) are not compatible with WH(WD). Ma and Balusubramanian[38] performed CASMCSCF calculations on WH and showed that this emission energy is reasonable for WH but that the vibrational analysis is incorrect and that the lower state frequency should be near 1897 cm^{-1}. This frequency is in agreement with our DFT calculations and experimental observation.

WH_2. A band at 1831.7 cm^{-1} appeared in our neon matrix on deposition and slightly increased on photolysis. This band shifts to 1323.9 cm^{-1} upon reaction with D_2 in neon and shows a 1.384 H/D isotopic frequency ratio. These two absorptions are assigned to the antisymmetric (b_2) stretching mode for WH_2 and WD_2, respectively. The experiments with $H_2 + D_2$ gave the same absorptions, whereas two new bands appeared at 1839.7 and 1330.3 cm^{-1} with HD, which are due to W−H and W−D stretching vibrations in the WHD molecule. DFT calculations predict bent WH_2 with a $^5B_2$ ground state and strong antisymmetric mode at 1920−1930 cm^{-1} using different methods (Table 3), which is in good agreement with the experimental value.

WH_3. The reaction of W with H_2 also revealed a new absorption at 1895.3 cm^{-1}, which increased slightly on sample annealing and decreased slightly on photolysis. The deuterium counterpart of this band was found at 1361.1 cm^{-1}, showing a 1.393 H/D isotopic frequency ratio. In HD experiments, a weak upper new band at 1901.2 cm^{-1} tracks with the 1895.3 cm^{-1} band, and the lower new band at 1363.6 cm^{-1} goes with the

1361.1 cm^{-1} band. This isotopic pattern is characteristic of a metal trihydrides species. DFT calculations were done for WH_3, and the calculated frequencies and isotopic distributions support the identification of the WH_3 molecule with C_{3v} symmetry. The antisymmetric degenerate (e) W−H stretching mode is predicted at 1932.9 cm^{-1} with BPW91 and at 1947.0 cm^{-1} with B3LYP functionals. This mode is computed to be 20-fold stronger than the symmetric (a_1) stretch, which is in accord with the fact that only one absorption is observed for WH_3. As for mixed H/D substitution of WH_3, upper and lower bands, respectively, computed between antisymmetric and symmetric stretching modes correspond to stretching vibrations in mixed WHD_2 and WH_2D molecules, which match the experimental values very well. Finally, the $(H_2)WH$ complex is 21.3 kcal/mol higher in energy and not expected to contribute to the spectrum. This contrasts $(H_2)AuH$, which is the stable structure.[28]

The absorption of WH_3 is also observed in argon matrixes at 1878.6 cm^{-1} and WD_3 at 1344.3 cm^{-1} with a 1.397 H/D frequency ratio. These bands increased on annealing, decreased on broadband photolysis, and increased on further annealing. Sharp new bands at 1883.5 and 1348.4 cm^{-1} with HD that exhibit similar behavior as the 1878.7 and 1343.4 cm^{-1} absorptions are clearly due to WH_2D and WHD_2.

WH_4. The sharp band at 1920.5 cm^{-1} with a site splitting at 1921.8 cm^{-1} is increased by 50% on annealing, decreased slightly on broadband photolysis, and increased by 100% on further annealing to 11 K. The deuterium counterpart at 1377.0 cm^{-1} with a site at 1377.8 cm^{-1} behaved likewise. These absorptions can be assigned to the antisymmetric (t_2) W−H and W−D stretching fundamentals of tetrahedral WH_4 and WD_4, respectively. In the HD experiments, two upper bands split to 1935.8 and 1920.2 cm^{-1} and two lower bands to 1384.8 and 1378.0 cm^{-1}. The $H_2 + D_2$ experiments gave the same absorptions as HD experiments. These four absorptions due to symmetric and antisymmetric WH_2 and WD_2 stretching fundamentals in WH_2D_2 show that a tetrahydride is formed and the same modes for HD and $H_2 + D_2$ argue for the tetrahedral structure.[25,26] The antisymmetric modes in WH_2D_2 are very close to the t_2 modes observed for WH_4 and WD_4, respectively, and the new symmetric modes lie higher by 15 cm^{-1} for the WH_2 mode and 8 cm^{-1} for the WD_2 mode in the WH_2D_2 molecule. A 50% weaker, similarly split 526.9, 525.2 cm^{-1} band tracked with the 1921.8, 1920.5 cm^{-1} absorption and can be assigned to the antisymmetric (t_2) deformation mode. The analogous tetrahedral metal hydrides, MH_4, were formed in reactions of laser-ablated Ti, Zr, and Hf atoms with molecular hydrogen in argon matrix experiments.[24−26]

DFT calculations support this assignment, and the results are summarized in Table 5. Calculations show that the WH_4 molecule has a triplet $^3A_1$ ground state with the tetrahedral structure using two functionals and two pseudopotentials. The predicted triply degenerate (t_2) antisymmetric W−H and W−D stretching modes with BPW91/6-311++G**/SDD are only 35 and 11 cm^{-1} higher, respectively, than experimental neon matrix values, whereas calculation with the same functional, basis sets, and the LANL2DZ pseudopotential gave essentially the same frequencies. The predicted symmetric stretching modes are about 14 cm^{-1} higher for WH_2 and 6 cm^{-1} for WD_2 subunits in the WH_2D_2 molecule, which are much closer to neon experimental separations of 16 and 7 cm^{-1}. Furthermore, the calculated intensities of the symmetric modes are half of those for the antisymmetric modes, which are in excellent agreement with experimental observations. Although the B3LYP functional gave about 20 cm^{-1} higher W−H stretching frequencies, the predicted H/D isotopic ratios and relative intensities match experimental values very well. The BPW91 calculation also predicted the deformation mode at 558.4 cm^{-1}, which is 31.5 cm^{-1} higher than observed and in satisfactory agreement.

WH_6. The 2004.4, 1953.8, 1927.5, 1080.3, and 840.7 cm^{-1} neon matrix absorptions are favored at higher H_2 concentrations (4% relative to 2% H_2 in neon) and higher laser energy. These five bands exhibit common behavior and band contour (Figure 2): they are observed on deposition, increased on annealing to 10 K, decreased by broadband photolysis, and increased on further annealing. When these five bands are most intense, a sixth weaker 2021.2 cm^{-1} band is associated. In deuterium experiments, counterparts at 1439.9, 1384.1, 779.2, and 609.1 cm^{-1} (Figure 3) give H/D frequency ratios of 1.392, 1.393, 1.386, and 1.380, respectively, which are near ratios for other tungsten hydride absorptions (no D counterparts are observed for the weakest 2021.2 and 1953.8 cm^{-1} peaks). With HD new 2003.4, 1953.4, 1927.5, and 1432.5 cm^{-1} bands in the upper region and one 797.9 cm^{-1} band in the lower region are observed for this product species.

BPW91 calculations predict a distorted trigonal prism C_{3v} symmetry global minimum $^1A_1$ state for WH_6, Figure 7, with three equivalent shorter W−H and three equivalent longer W−H bonds, in agreement with previous work,[16−18] but the B3LYP functional finds the C_{5v} parachute structure in a dead heat (Table 7). However, the observed spectrum for WH_6 described above can be used to determine the structure by matching calculated spectra for different structures.

First, the observation of four W−H stretching modes for WH_6 rules out the octahedral structure, which has one triply degenerate stretching mode. Second, the C_{5v} parachute structure has two strong W−H stretching modes and no strong deformation mode near 1100 cm^{-1}, which is not compatible with the observed spectrum. Third, the C_{5v} umbrella has one strong W−H stretching mode and also can be eliminated. The C_{3v} hemisphere (called C_{3v}-B by earlier workers)[16,18] is 6−13 kcal/mol higher in energy than the distorted prism global minimum depending upon the calculation (refs 16−18 and this work), but the frequencies calculated here are a reasonable match for the observed spectrum except for the higher a_1 and e stretching modes, which are predicted to be 73−74 cm^{-1} higher by BPW91 than observed. These frequencies computed for the C_{3v} prism are only 36−38 cm^{-1} higher than observed. On this basis, our DFT frequencies for the C_{3v} prism fit the observed values better.

The distorted C_{3v} prism WH_6 structure contains three equivalent shorter W−H and three equivalent longer W−H bonds, and the two higher DFT calculated W−H stretching frequencies, a_1 and e modes, are predominantly due to the shorter trio of W−H bonds and the next two a_1 and e modes to the longer W−H bond trio based on computed displacement coordinates for each mode. The four W−H stretching modes are calculated at 2059.3, 2039.9, 1963.7, and 1949.8 cm^{-1}, respectively, with the BPW91 functional (Table 7) as weak a_1, strong e, weak a_1, and strong e modes, which are 10−38 cm^{-1} (0.5−2%) higher but in excellent agreement with the observed 2021.2, 2004.4, 1953.8, and 1927.5 cm^{-1} bands. The intensities of the symmetric (a_1) modes are overestimated by the calculation relative to the antisymmetric (e) modes. In addition, the next most intense a_1 and e deformation modes computed at 1151.1 and 894.0 cm^{-1} are observed at 1080.3 and 840.7 cm^{-1} in almost as good agreement. The B3LYP functional predicts slightly higher frequencies with the same intensity profile. In conclusion, the overall excellent agreement between six calculated and observed frequencies for the distorted C_{3v} prism WH_6 structure

confirms the identification, assignments, and structure of the novel WH_6 molecule observed in these experiments. We note that the SCF all-electron computed frequencies for the C_{3v} prism[16] are slightly higher but also in good agreement with the observed frequencies.

Only the strongest band of WH_6 is observed in solid argon, at 1923.7 cm^{-1}, and WD_6 was not made in pure D_2 where the yield of WD_4 was very small. Apparently, matrix cavity size plays a role in the formation of WH_6.

For the WH_3D_3 isotopic molecule produced in the HD experiments, there are four possible isotopic modifications; however, the isomer with the shorter three W−D bonds is slightly lower in energy as determined from zero-point energy corrections. Four frequencies for this isomer are observed in our HD spectra at 1952.6, 1927.5, 1432.5, and 797.9 cm^{-1} in agreement with bands calculated at 1964.3, 1952.4, 1443.2, and 833.6 cm^{-1}. In addition, a very weak 2003.4 cm^{-1} band is due to the shorter three W−H bonded isomer, but the stronger band is masked by the 1384.8 cm^{-1} band of WH_2D_2. It is possible that the WH_2DH_2D and WHD_2HD_2 isomers are observed, but if so, the bands are much weaker (for example the 1932 cm^{-1} band in Figure 4d). Our HD spectra suggest that the more stable WD_3(short) H_3(long) isomer is favored, which provides further evidence for the fluxional nature of WH_6. The dynamics of formation of WH_4 and WH_6 from WH_2 appear to be sensitive to the local environment. It is perhaps surprising that little WD_4 (triplet state) and no WD_6 (singlet state) are formed in pure deuterium where the major product appears to be slightly perturbed WD_2 in the presumably high-spin quintet $WD_2(D_2)_x$ complex.

[WH_4], i.e., $(WH_4)(Ne)_x(H_2)$. The new bands at 1911.5 and 1909.9 cm^{-1} display opposite behavior from the absorptions assigned to WH_6 in that they decrease slightly on annealing to 8 K and virtually disappear on annealing to 10 K but increase 3-fold on broadband photolysis and then disappear again on further annealing to 11 K when WH_4 and WH_6 increase. A weak band at 1925.7 cm^{-1} (partly overlapped by the 1927.5 cm^{-1} WH_6 band) exhibits the same behavior as the 1911.5 cm^{-1} band. In the lower frequency region, an almost identical new doublet observed at 515.6 and 514.0 cm^{-1} tracks with the upper doublets. The upper doublets shift to 1371.2 and 1370.3 cm^{-1} with D_2 and give a 1.394 H/D frequency ratio. Unfortunately the deuterium counterpart of 1925.7 cm^{-1} is not resolved from the stronger 1371.2, 1370.3 cm^{-1} band, and counterparts of 515.6 and 514.0 cm^{-1} shift below our measurable region. It is interesting to note that HD experiments give nearly the same upper absorptions at 1909.7 and 1371.2 cm^{-1} as the H_2 and D_2 reagents.

These bands appear to be produced from photodissociation of WH_6, so $WH_4(H_2)$ and $WH_2(H_2)_2$ complexes were calculated by DFT: the former attempts failed to converge on singlet and triplet surfaces, but the latter triplet complex is stable although 26.0 kcal/mol higher in energy than WH_6. For the $WH_2(H_2)_2$ complex, the BPW91 functional predicts the stronger antisymmetric W−H_2 stretching and W−$(H_2)_2$ stretching modes at 1941.5 and 456.9 cm^{-1}, respectively, the weaker symmetric W−H_2 mode at 1944.2 cm^{-1}, and the strong H−H stretching mode at 2336.7 cm^{-1}. This complex was suggested in our preliminary communication.[29] An obvious problem with this assignment is the failure to observe an H−H stretching mode although such mode intensities tend to be overestimated by DFT computations, and the bands are broad and more difficult to observe.[22] In addition, the calculation predicts the low-frequency mode 58.7 cm^{-1} too low, which is opposite the normal discrepancy between calculated and observed frequencies.

Furthermore, the behavior of the 1911.5, 1909.0 cm^{-1} and 515.6, 514.0 cm^{-1} bands is unique: marked growth on photolysis but disappearance on annealing to 10 K. We must note the striking relationship of the above bands to WH_4 absorptions at 1921.8, 1920.5 cm^{-1} and 526.9, 525.2 cm^{-1}, which is a small 10 cm^{-1} red shift. Hence, the above bands could be due to perturbed WH_4 where the symmetric mode is weakly observed, i.e., the weak 1925.7 cm^{-1} absorption, and this is the most likely identification. Upon photodissociation WH_6 eliminates H_2 to form perturbed WH_4 where H_2 is trapped with neon atoms separating WH_4 and H_2. On annealing the solid above 8 K, neon atoms diffuse and WH_6 reforms. This is consistent with our experience that diffusion of trapped species in solid neon requires warming above 8 K (solid neon can be maintained on brief annealing to 12 K).[27,28]

$$WH_6(^1A_1, C_{3v}) \xrightarrow[\text{neon, 4 K}]{240-700\text{ nm}} (WH_4)(Ne)_x(H_2) \xrightarrow[\text{neon, 10 K}]{\text{anneal}} WH_6$$

Other Absorptions. The absorption at 995.8 cm^{-1} appears to be favored at higher laser energy, and it shifts to 716.4 cm^{-1} with D_2 for a 1.390 isotopic frequency ratio. The lower frequency suggests a bridged W−H−W vibration, and rhombic W_2H_2 structures were computed. A high spin $^{11}B_{1u}$ rhombic structure (W−H, 1.934 Å; W−W, 2.883 Å) appears to be the global minimum. The observed frequency is near the strongest computed mode (b_{2u}) at 928 cm^{-1}, which supports a bridged W−H−W bond and a possible assignment to W_2H_2, but absorption could also be due to a bridged W_xH species. It is interesting to note that dihydrogen dissociates on W {110}, and the hydrogen adatom occupies a W−H−W short bridge site.[47] Vibrational frequencies near 1290 and 1050 cm^{-1} have been assigned to this feature and the W−H bond length measured as 1.95 Å.[47,48] This W−H−W bridge bond characterization supports our postulate of open bridged tungsten hydride species in the 990 cm^{-1} spectral region. Finally, broad neon matrix bands at 1786 and 1735 cm^{-1} are due to tungsten cluster terminal hydride species denoted W_xH_y. Counterparts of these bands are even observed in pure deuterium (Figure 5).

The argon matrix experiments give a different product distribution from neon. The straightforward assignment to WH_2 in solid argon is the weak 1816.8 cm^{-1} band. The stronger split 1866.2, 1865.1 cm^{-1} feature shifts to 1337.0 cm^{-1} with D_2 (ratio 1.395) and to 1865.7 and 1338.0 cm^{-1} with HD, which are characteristic of a WH_2 like mode. Because unsaturated tungsten complexes can weakly bind argon as a ligand $W(CO)_5(Ar)$,[49−51] it is possible that the 1866.2 cm^{-1} absorption is due to a WH_2-$(Ar)_x$ complex. However, the more likely identification is a higher dihydrogen complex $(H_2)_xWH_2$, but we cannot be certain. If WH_4 is formed in solid argon, the weak, broad 1911 cm^{-1} absorption provides the only evidence. On the other hand, the 1923.7 cm^{-1} argon matrix absorption behaves like WH_6 and shows only a 3.8 cm^{-1} shift from neon for this *saturated* tungsten hexahydride.

Reaction Mechanisms. Insertion of ground-state tungsten into H_2 to form WH_2, reaction 1, is exothermic by 22.2 kcal/mol at the BPW91 level and by 19.4 kcal/mol at the MRSDCI level.[39] However, the absorption assigned to WH_2 was observed after deposition but decreased on annealing, indicating that the insertion reaction of ground-state tungsten into H_2 is not spontaneous. This result is in agreement with theoretical calculations, which suggested that the ^7S ground state of the W atom must surmount a large 28 kcal/mol barrier for insertion

into H_2.[39] This insertion barrier is reduced markedly for the ^5D electronic state of the W atom with H_2. The energy required for a tungsten atom inserting into H_2 is provided by the laser ablation process and by broadband photolysis.[52] The WH_2 species further reacts with H_2 to give WH_4 and WH_6, and both reactions 2 and 3 are exothermic, by 27.0 and 14.6 kcal/mol,[51] respectively. These exothermic reactions proceed spontaneously on annealing in the 8−11 K neon matrix and show no significant activation energy requirement. We note that the C_{5v} parachute structure has almost the same energy as the C_{3v} ground-state WH_6 molecule. The exothermicity of reaction 3 is more than enough to populate this C_{5v} structure, which provides a ready means of H/D position exchange or fluxional behavior for the ground-state WH_6 molecule. Finally, WH_6 photodissociates with 240−700 nm radiation, but WH_6 reforms on further annealing, reaction 4.

$$W(^7S) + H_2\,(^1\Sigma_g^+) \rightarrow WH_2\,(^5B_2)\ \Delta E = -22.2\ \text{kcal/mol} \quad (1)$$

$$WH_2\,(^5B_2) + H_2\,(^1\Sigma_g^+) \rightarrow WH_4\,(^3A_1)\ \Delta E = -27.0\ \text{kcal/mol} \quad (2)$$

$$WH_4\,(^3A_1) + H_2\,(^1\Sigma_g^+) \rightarrow WH_6\,(^1A_1)\ \Delta E = -14.6\ \text{kcal/mol} \quad (3)$$

$$WH_6\,(^1A_1) \xrightarrow{240-700\ \text{nm}} (WH_4)(Ne)_x(H_2) \xrightarrow{8-10\ \text{K}} WH_6 \quad (4)$$

In the laser ablation process, the endothermic reaction of W atoms with H_2 gives WH and atomic hydrogen, and WH species are trapped in the low-temperature matrix. Some WH_2 is made by the H + WH reaction as WH_2 and WD_2 are observed with HD and WHD is found with the $H_2 + D_2$ reagent mixture. On sample annealing, WH further adds H_2 to form WH_3, which is exothermic by 23.9 kcal/mol. The WH_5 species was not detected in these experiments although the reaction of WH_3 and H_2 is exothermic. It is likely that WH_5 is not observed due to spectral congestion or that most of the H_2 is consumed in other more favorable reactions.

$$W(^7S) + H_2\,(^1\Sigma_g^+) \rightarrow WH\,(^6\Sigma^+) + H\ \Delta E = 38.7\ \text{kcal/mol} \quad (5)$$

$$WH\,(^6\Sigma) + H_2\,(^1\Sigma_g^+) \rightarrow WH_3\,(^4A_1)\ \Delta E = -23.9\ \text{kcal/mol} \quad (6)$$

$$WH_3\,(^4A_1) + H_2\,(^1\Sigma_g^+) \rightarrow WH_5\,(^2A')\ \Delta E = -17.3\ \text{kcal/mol} \quad (7)$$

Conclusions

Reactions of laser-ablated tungsten atoms with molecular hydrogen during co-deposition in excess neon at 3.5 K produced a series of novel tungsten hydrides. WH, WH_2, and WH_3 appear in solid neon at 1860.2, 1831.9, and 1894.6 cm^{-1}, respectively. Absorptions due to WH_4 at 1920.1 and 526.9 cm^{-1} increased on annealing. A group of new absorptions at 2021.2, 2004.4, 1953.8, 1927.5, 1080.3, and 840.7 cm^{-1} are assigned to the hexahydride WH_6, which is found by calculations[15−18] to be a closed-shell trigonal prism with C_{3v} symmetry. The bands of WH_6 increase on annealing, decrease on broadband photolysis, and increase on further annealing. The insertion reaction of ground-state tungsten into H_2 is not spontaneous, which is in agreement with the theoretical calculations of any energy barrier for insertion.[39] However, WH_2 reacts further with H_2 to give WH_4 and WH_6, which proceed spontaneously on annealing in the solid neon matrix and show no significant activation energy. WH_6 photodissociates to WH_4 but reforms on further annealing to 10 K. However, WD_6 is not produced in solid deuterium where the major product is the high spin $WD_2(D_2)_x$ complex.

The identification of WH_6 in these experiments and the confirmation of its unusual C_{3v} prism structure predicted by theory[15−18] is made possible by excellent agreement between DFT calculated and neon matrix observed frequencies for four W−H stretching (two a_1 and two e) and two W−H deformation (a_1 and e) modes. Recent quantitative agreement between experiment[14] and theory[15] for $W(CH_3)_6$ reinforces the theoretical predictions for WH_6. The only other metal hexahydride known is ReH_6^{3-} in the K_3ReH_6 solid, and this anion has the regular octahedral structure.[54,55]

Acknowledgment. We gratefully acknowledge support from N.S.F. Grant CHE 00-78836.

References and Notes

(1) Bullock, R. M.; Song, J.-S. *J. Am. Chem. Soc.* **1994**, *116*, 8602.
(2) Luan, L.; Song, J.-S.; Bullock, R. M. *J. Org. Chem.* **1995**, *60*, 7170.
(3) Cheng, T.-Y.; Bullock, R. M. *J. Am. Chem. Soc.* **1999**, *121*, 3150.
(4) Chi, Y.; Chuang, S. H.; Liu, L. K.; Wen, Y. S. *Organometallics* **1991**, *10*, 2485.
(5) (a) Kubas, G. J.; Ryan, R. R.; Swanson, B. I.; Vergamini, P. J.; Wasserman, H. J. *J. Am. Chem. Soc.* **1984**, *106*, 451. (b) Kubas, G. J.; Ryan, R. P.; Wrobleski, D. A. *J. Am. Chem. Soc.* **1986**, *108*, 1339.
(6) (a) Upmacis, R. K.; Poliakoff, M.; Turner, J. J. *J. Am. Chem. Soc.* **1986**, *108*, 3645. (b) Jackson, S. A.; Hodges, P. M.; Poliakoff, M.; Turner, J. J.; Grevels, F. W. *J. Am. Chem. Soc.* **1990**, *112*, 1221.
(7) Saillard, J.-Y.; Hoffmann, R. *J. Am. Chem. Soc.* **1984**, *106*, 2006 and references therein.
(8) King, A. D.; King, R. B.; Yang, D. B. *J. Am. Chem. Soc.* **1981**, *103*, 2699.
(9) Jean, Y.; Eisenstein, O.; Volatron, F.; Maouche, B.; Sefta, F. *J. Am. Chem. Soc.* **1986**, *108*, 6587.
(10) Ishikawa, Y.-I.; Hackett, P. A.; Rayner, D. M. *J. Phys. Chem.* **1989**, *93*, 652.
(11) Shortland, A. J.; Wilkinson, G. *J. Chem. Soc., Dalton Trans.* **1973**, 872.
(12) Gillespie, R. J.; Nyholm, R. S. *Q. Rev. Chem. Soc.* **1957**, *11*, 339.
(13) Haaland, A.; Hammel, A.; Rypdal, K.; Volden, H. V. *J. Am. Chem. Soc.* **1990**, *112*, 4547.
(14) Pfennig, V.; Seppelt, K. *Science* **1996**, *271*, 626.
(15) Kaupp, M. *J. Am. Chem. Soc.* **1996**, *118*, 3018.
(16) Shen, M.; Schaefer, H. F., III.; Partridge, H. *J. Chem. Phys.* **1993**, *98*, 508.
(17) Kang, S. K.; Tang, H.; Albright, T. A. *J. Am. Chem. Soc.* **1993**, *115*, 1971.
(18) Tanpipat, N.; Baker, J. *J. Phys. Chem.* **1996**, *100*, 19818.
(19) Van Zee, R. J.; DeVore, T. C.; Weltner, W., Jr. *J. Chem. Phys.* **1979**, *71*, 2051. (Mo + H_2).
(20) Xiao, Z. L.; Hauge, R. H.; Margrave, J. L. *J. Phys. Chem.* **1992**, *96*, 636. (Cr, Mo + H_2).
(21) Andrews, L.; Manceron, L.; Alikhani, M. E.; Wang, X. *J. Am. Chem. Soc.* **2000**, *122*, 11011. (Pd + H_2).
(22) Andrews, L.; Wang, X.; Alikhani, M. E.; Manceron, L. *J. Phys. Chem. A* **2001**, *105*, 3052. (Pd + H_2).
(23) Andrews, L.; Wang, X.; Manceron, L. *J. Chem. Phys.* **2001**, *114*, 1559. (Pt + H_2).
(24) Chertihin, G. V.; Andrews, L. *J, Am. Chem. Soc.* **1994**, *116*, 8322. (Ti + H_2).
(25) Chertihin, G. V.; Andrews, L. *J. Am. Chem. Soc.* **1995**, *117*, 6402. (Zr, Hf + H_2).
(26) Chertihin, G. V.; Andrews, L. *J. Phys. Chem.* **1995**, *99*, 15004. (Zr, Hf + H_2).
(27) Wang, X.; Andrews *J. Phys. Chem. A* **2002**, *106*, 3706. (Rh + H_2).
(28) Wang, X.; Andrews, L. *J. Am. Chem. Soc.* **2001**, *123*, 12899. (Au + H_2).
(29) Wang, X.; Andrews, L. *J. Am. Chem. Soc.* **2002**, *124*, 5636.

(30) Burkholder, T. R.; Andrews, L. *J. Chem. Phys*. **1991**, *95*, 8697. Hassanzadeh, P.; Andrews, L. *J. Phys. Chem*. **1992**, *96*, 9177.

(31) Zhou, M.; Andrews, L. *J. Chem. Phys*. **1999**, *111*, 4230.

(32) Frisch, M. J.; Trucks, G. W.; Schlegel, H. B.; Scuseria, G. E.; Robb, M. A.; Cheeseman, J. R.; Zakrzewski, V. G.; Montgomery, J. A., Jr.; Stratmann, R. E.; Burant, J. C.; Dapprich, S.; Millam, J. M.; Daniels, A. D.; Kudin, K. N.; Strain, M. C.; Farkas, O.; Tomasi, J.; Barone, V.; Cossi, M.; Cammi, R.; Mennucci, B.; Pomelli, C.; Adamo, C.; Clifford, S.; Ochterski, J.; Petersson, G. A.; Ayala, P. Y.; Cui, Q.; Morokuma, K.; Malick, D. K.; Rabuck, A. D.; Raghavachari, K.; Foresman, J. B.; Cioslowski, J.; Ortiz, J. V.; Stefanov, B. B.; Liu, G.; Liashenko, A.; Piskorz, P.; Komaromi, I.; Gomperts, R.; Martin, R. L.; Fox, D. J.; Keith, T.; Al-Laham, M. A.; Peng, C. Y.; Nanayakkara, A.; Gonzalez, C.; Challacombe, M.; Gill, P. M. W.; Johnson, B. G.; Chen, W.; Wong, M. W.; Andres, J. L.; Head-Gordon, M.; Replogle, E. S.; Pople, J. A. *Gaussian 98*, revision A.6; Gaussian, Inc.: Pittsburgh, PA, 1998.

(33) (a) Becke, A. D. *J. Chem. Phys.* **1993**, *98*, 5648. (b) Lee, C.; Yang, W.; Parr, R. G. *Phys. Rev. B* **1988**, *37*, 785.

(34) (a) Becke, A. D. *Phys. Rev. A* **1988**, *38*, 3098. (b) Perdew, J. P.; Wang, Y. *Phys. Rev. B* **1992**, *45*, 13244.

(35) (a) Krishnan, R.; Binkley, J. S.; Seeger, R.; Pople, J. A. *J. Chem. Phys.* **1980**, *72*, 650. (b) Frisch, M. J.; Pople, J. A.; Binkley, J. S. *J. Chem. Phys.* **1984**, *80*, 3265.

(36) (a) Wadt, W. R.; Hay, P. J. *J. Chem. Phys.* **1985**, *82*, 284. (b) Hay, P. J.; Wadt, W. R. *J. Chem. Phys.* **1985**, *82*, 299.

(37) Andrae, D.; Haussermann, U.; Dolg, M.; Stoll, H.; Preuss, H. *Theor. Chim. Acta* **1990**, *77*, 123.

(38) Ma, Z.; Balusubramanian, K. *Chem. Phys. Lett.* **1991**, *181*, 467.

(39) Balasubramanian, K.; Ma, Z. *J. Phys. Chem*. **1991**, *95*, 9794.

(40) Deleeuw, B. J.; Yamaguchi, Y.; Schaefer, H. F., III. *Mol. Phys*. **1995**, *84*, 1109.

(41) Ma, B.; Collins, C. L.; Schaefer, H. F. *J. Am. Chem. Soc*. **1996**, *118*, 870.

(42) Bauschlicher, C. W., Jr.; Ram, R. S.; Bernath, P. F.; Parsons, C. G.; Galehouse, D. *J. Chem. Phys*. **2001**, *115*, 1312.

(43) Balabanov, N. B.; Boggs, J. E. *J. Phys. Chem. A* **2000**, *104*, 7370.

(44) Bayse, C. A.; Hall, M. B. *J. Am. Chem. Soc*. **1999**, *121*, 1348.

(45) Jacox, M. E. *Chem. Phys.* **1994**, *189*, 149.

(46) Garvey, J. F.; Kuppermann, A. *J. Phys. Chem.* **1988**, *92*, 4583.

(47) Willis, R. F. *Surf. Sci*. **1979**, *89*, 457 and references therein.

(48) Smith, K. E.; Kevan, S. D. *Phys. Rev. Lett.* **1990**, *64*, 567.

(49) Wells, J. R.; Weitz, E. *J. Am. Chem. Soc.* **1992**, *114*, 2783.

(50) Sun, X.-Z.; George, M. W.; Kazarian, S. G.; Nikiforov, S. M.; Poliakoff, M. *J. Am. Chem. Soc.* **1996**, *118*, 10525.

(51) Ehlers, A. W.; Frenking, G.; Baerends, E. J. *Organometallics* **1997**, *16*, 4896.

(52) Kang, H.; Beauchamp, J. L. *J. Phys. Chem*. **1985**, *89*, 3364.

(53) Energy calcualtions at BPW91/6-311++G**/SDD level of theory.

(54) Bronger, W.; Auffermann, G. A.; Schilder, H. *Z. Anorg. Allg. Chem.* **1998**, *624*, 497.

(55) King, R. B. *Coord. Chem. Rev.* **2000**, *813*, 200−202.